Bull. Chem. Soc. Ethiop. **2024**, 38(3), 685-699.
DOI: https://dx.doi.org/10.4314/bcse.v38i3.11

ISSN 1011-3924
Printed in Ethiopia
Online ISSN 1726-801X

ENOXACIN FLUOROQUINOLONE ANTIBACTERIAL AGENT COMPLEXES WITH Pt(IV), Ru(III) AND Ir(III) IONS: SYNTHESIS, SPECTROSCOPIC, PHYSICOCHEMICAL CHARACTERIZATIONS AND BIOLOGICAL STUDIES

Abeer A. El-Habeeb[1] and Moamen S. Refat[2*]

[1]Department of Chemistry, College of Science, Princess Nourah bint Abdulrahman University, P.O. Box 84428, Riyadh 11671, Saudi Arabia
[2]Department of Chemistry, College of Science, Taif University, P.O. Box 11099, Taif 21944, Saudi Arabia

(Received December 23, 2023; Revised January 26, 2024; Accepted January 30, 2024)

ABSTRACT. The synthesis, physicochemical characterizations, and biological investigations on the chelation of the antibiotic medication enoxacin (EXN) with certain vital metal ions, such as platinum(IV), ruthenium(III), and iridium(III) are discussed in this study. These compounds structures were interpreted based on elemental analysis and spectral measurements (FTIR, ^{1}H-NMR, UV-Vis electronic, and XRD). The findings show that there is same coordination pathway for the chelation behavior of enoxacin complexes: a monodentate manner. The Pt(IV), Ru(III), and Ir(III) complexes are coordinated through the N atom of the piperazine ring, which is an unusual mode of coordination for this class of compounds. The dissolved complexes in DMSO were found to have non-electrolyte nature based on their molar conductance measurements. The formula for these complexes is $[Pt(EXN)_3(H_2O)_2Cl]$ (**1**), $[Ru(EXN)_3(H_2O)_3]$ (**2**), and $[Ir(EXN)_3(H_2O)_3]$ (**3**). Using scanning electron microscope (SEM) analysis and X-ray powder diffraction (XRD), the nano-scale range of the Pt(IV), Ru(III), and Ir(III) complexes has been determined. Results of *in vitro* cytotoxicity were examined using MCF-7 cells (human breast cancer cell line) and HepG-2 cells (human hepatocellular carcinoma) that had been grown. The cytotoxic activity of the metal complexes demonstrated a cytotoxic effect against the growth of human breast and liver cancer cell lines.

KEY WORDS: Enoxacin, Platinum(IV), Complexity, Spectral analyses, Biological assessments

INTRODUCTION

The antibacterial activity may be dependent on the chelation of the metal ion with the carbonyl and carboxyl groups of the quinolones and the binding of the resultant complex to DNA [1, 2]. Thus, a plethora of research on the interaction between metal cations and quinolone series has been described and evaluated in the literature [3-8]. Research has demonstrated that metal complexes have promising antibacterial, antioxidant, anti-tumor, and antidiabetic properties [9, 10]. Because of their anticancer properties, metal complexes have been extensively studied in recent years and have had a significant impact on cancer chemotherapy. Because cancer is becoming a greater hazard to human health, cisplatin is one of the most significant discoveries among them [11-13]. As of right now, cisplatin and additional platinum-based substances including carboplatin and oxaliplatin are effective against a few cancer kinds [14]. Nevertheless, during treating cancer, these medications are linked to dose-limiting adverse effects such as ototoxicity, nephrotoxicity, neurotoxicity, and emetogenesis; additionally, with time, resistance limits their effectiveness [15]. These drawbacks have prompted a thorough search for and development of substitute substances that bind to nucleic acids non-covalently and may be used as anticancer medications. The compounds based on Au, Pt, Ru, Pd, Os, Ir, and Cu have been studied the most in this context and offer promising potential as effective substitutes for the medication cisplatin [16-19].

*Corresponding author. E-mail: moamen@tu.edu.sa ; msrefat@yahoo.com

One of the second-generation quinolone antibiotics, enoxacin (EXN) (Formula I), has a piperazinyl moiety in position C-7 and is fluorinated in position C-6. By preventing DNA replication and transcription and suppressing cell DNA gyrase, it eradicates germs [20, 21]. Because enoxacin has strong cytotoxic activity, it is a very effective treatment for tumors [22]. There have been reports of enoxacin complexes with Cu(II), Zn(II), Cd(II), Ni(II), Co(II), Mn(II), and Ag(I) [23-26].The findings suggested that metal ion coordination may boost medicinal compounds' antibacterial activity and enhance their overall activity. The chelation of metal atoms with neighbouring 4-oxo and carboxyl groups is the suggested mechanism of metal-enoxacin interaction.

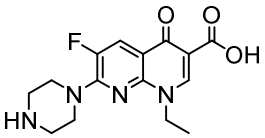

Formula I. enoxacin (EXN) drug.

Metal chelates containing quinolones have the capacity to bind with different metal ions and exhibit biological action towards diverse microorganisms [27-30]. Quinolones have the ability to function as bridging, bidentate, and unidentate chelates. Quinolones are typically coordinated in a bidentate manner; this occurs when the COOH group and carbonyl oxygen atom deprotonate, resulting in the loss of one oxygen atom. Quinolones can, on rare occasions, function as bidentate chelates by passing through both piperazinic and carboxyl nitrogen atoms. Quinolones can also bind to metal ions through terminal piperazinyl nitrogen to form complexes as unidentate ligands [30].

As far as the literature review goes, there have not been any published investigations on the relationship between enoxacin and some transition metals of biological interest, such as Pt(IV), Ru(III), and Ir(III). In order to introduce our work, we have focused on this topic. This time, we concentrated on the following: (i) how the quinolone-antibacterial drug enoxacin interacts with Pt, Ru, and Ir metals; (ii) how the newly formed complexes are characterized using various spectroscopy techniques; (iii) how the complexes' antibacterial activity is measured using the minimum inhibitory concentration (MIC) against four different microorganisms; and (iv) how the synthesis of enoxacin-based complexes may be used to treat cancer.

EXPERIMENTAL

Chemical

The supplier of enoxacin (EXN) was Aldrich Sigma Chemical Company. The Fluka Chemical Company supplied the $RuCl_3$, $H_2PtCl_6.6H_2O$, and $IrCl_3.xH_2O$ along with solvents such CH_3OH and dimethylsulfoxide (DMSO), which were utilized without additional purification.

Instrumentations

With the use of a Perkin Elmer CHN 2400 (USA), the percentages of %C, %H, and %N were quantified microanalytically. The metal contents (%) were calculated using standard gravimetric analytical techniques. Using a Jenway 4010 conductivity meter, the complexes' molar conductivities (1.0×10^{-3} mol/cm^3) in DMSO were measured. The electronic spectra of the produced metal complexes were recorded using a UV2 Unicam UV/Vis spectrophotometer that was equipped with a quartz cell that had a path length of 1.0 cm. Using KBr discs, infrared spectra were captured using a Bruker FT-IR Spectrophotometer (4000–400 cm^{-1}). Thermal measurements

(TG/DTG–50H) were recorded using a single loose top loading platinum sample pan under nitrogen atmosphere at a flow rate of 30 ml/min and a heating rate of 10 °C/min in the temperature range of 25–800 °C. The Shimadzu thermo gravimetric analyser under N_2 at 800 ºC was utilized for this purpose. Using TMS as the internal standard, ^{1}H-NMR spectra were captured in DMSO solutions using a Bruker 600 MHz spectrometer. The scanning electron microscope (SEM) pictures of the complexes were captured using a Jeol Jem-1200 EX II at an acceleration voltage of 25 kV. The samples' X-ray diffraction (XRD) patterns were recorded using $CuK_{\alpha 1}$ radiation and an X Pert Philips X-ray diffractometer with a graphite monochromator set to a scanning rate of 0.02 º/min (3 - 70 degrees). Using a JEOL 100s microscope, transmission electron microscopy (TEM) pictures were captured. Using a Gouy magnetic balance, the mass susceptibility (X_g) of the complexes was determined at room temperature. As previously reported, the effective magnetic moment (μ_{eff}) value was measured.

Synthesis of enoxacin complexes

An aqueous solution containing 20 mL of $H_2PtCl_6.6H_2O$ (1 mmol, 0.337 g), $RuCl_3$ (1 mmol, 0.208 g), and $IrCl_3.xH_2O$ (1 mmol, 0.299 g) was combined with a hot methanolic solution (3 mmol, 20 mL) of enoxacin (0.960 g). However, the three compounds were formed as a result of adding a few drops of aqueous ammonia to the EXN aliquot. The reaction mixtures were refluxed for three hours at approximately 75 ºC. After being filtered, the solutions were allowed to slowly evaporate. Following a day, microcrystalline products ranging in colour from yellow to dark brown were deposited, filtered, cleaned with methanol, and vacuum dried.

*[Pt(EXN)$_3$(H$_2$O)$_2$Cl] (**1**) complex*. The complex is yellow colour, soluble in (DMSO and DMF) and is a non-electrolyte (10 mS). Complex (**1**) ($C_{45}H_{52}ClF_3N_{12}O_{11}Pt$) (MW = 1224.6 g/mol): Yield: 77%. Calcd.: C, 44.10; H, 4.25; N, 13.72. Found: C, 43.97; H, 4.02; N, 13.59%.

*[Ru(EXN)$_3$(H$_2$O)$_3$] (**2**) complex*. The complex is dark brown, soluble in (DMSO and DMF) and is a non-electrolyte (7 mS). Complex (**2**) ($C_{45}H_{54}F_3N_{12}O_{12}Ru$) (MW = 1113.5 g/mol): Yield: 75%. Calcd.: C, 48.49; H, 4.85; N, 15.09. Found: C, 48.40; H, 4.77; N, 14.96%.

*[Ir(EXN)$_3$(H$_2$O)$_3$] (**3**) complex*. The complex is dark brown colour, soluble in (DMSO and DMF) and is a non-electrolyte (9 mS). Complex (**3**) ($C_{45}H_{54}F_3N_{12}O_{12}Ir$) (MW = 1150.3 g/mol): Yield: 79%. Calcd.: C, 46.94; H, 4.69; N, 14.60. Found: C, 46.85; H, 4.63; N, 14.42%.

Antibacterial assessment

Using the agar well diffusion method, the antibacterial activity of the ligand and complexes was ascertained [31]. Investigations were conducted on strains of four different bacterial species: G(+) (*Bacillus subtilis* and *Staphylococcus Aureus*) and G(-) (*Pseudomonas aeruginosa* and *Escherichia coli*). The typical antibacterial agent employed was ampicillin.

RESULTS AND DISCUSSION

Microanalytical and molar conductance investigation

The objective of this study was to synthesize, characterize chemically and biologically Ru(III), Pt(IV), and Ir(III) complexes with enoxacin as a second generation of floroquinolone medications. Finding the chelation mechanism under the effect of the mixed solvent CH_3OH/H_2O (50/10 v/v) was the primary goal of this investigation. The general formulae of three new EXN complexes as well as the percentages of the important elements (C, H, and N) coincide [M(EXN)$_3$(H$_2$O)$_3$] ((**2**

and **3**) M = Ru^{3+} and Ir^{3+}; $[Pt(EXN)_3(H_2O)_2Cl]$ (**1**) (Figure 1). The EXN complexes have higher melting points than 300 °C and are stable in air. Complexes **1-3** exhibit conductance data that falls within the non-electrolytic range (7–10 mS), with a low limit that can be compared to electrolyte materials as a point of reference [32]. Based on the conductance readings as well as checking by silver nitrate reagent, it is inferred that there are no chlorine atoms or that they are present inside the chelation sphere.

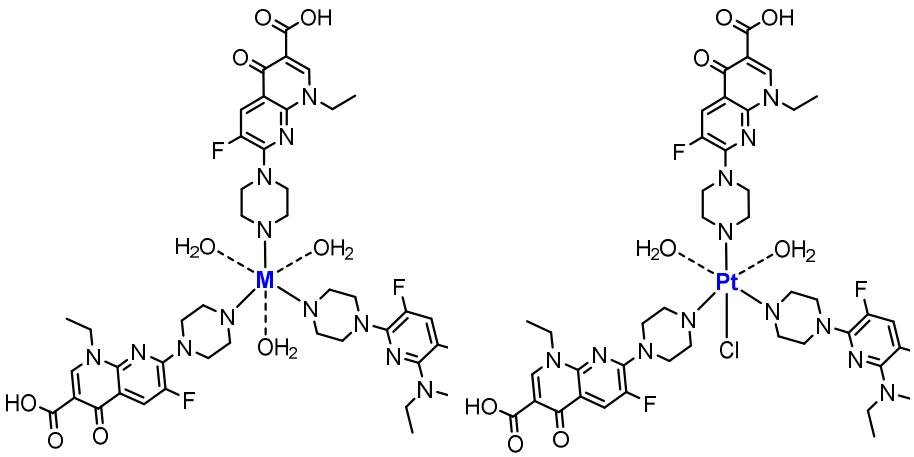

I **II**

Figure 1. Suggested structures of (**I**): M = (Ru^{3+} and Ir^{3+})–enoxacin and (**II**): Pt^{4+}–enoxacin complexes.

Infrared spectra

In order to explore the coordination modes in three different Ru^{3+}, Pt^{4+}, and Ir^{3+} metal ions, the FTIR spectra of Ru(III), Pt(IV), and Ir(III) EXN complexes **1-3** were compared with free EXN (Figure 2 and Table 1). At wavenumber ~1690 cm^{-1}, the free EXN-free drug's FTIR spectra displays a distinctive stretching vibration band called $\nu(C{=}O)_{COOH}$. The remaining distinct bands, located at 1620 and 2970 cm^{-1}, are attributed to the stretching vibrations of $\nu(C{=}O)_{pyridine}$ and $\nu(NH)_{piperazyl}$, respectively [33]. Because nitrogen is less electronegative than oxygen, a N–H bond is less polar than an O–H bond. As a result, the peak will be narrower and the N–H stretch will be less severe due to weaker hydrogen bonds. The ν(NH) piperazyl band disappears after chelation towards Ru^{3+}, Pt^{4+}, and Ir^{3+} metal ions (complexes **1-3**). The characteristic band caused by $\nu(C{=}O)_{COOH}$ at 1618–1613 cm^{-1} remains unshifted, and the stretching vibration band of $\nu(C{=}O)_{COOH}$ is shifted to a higher wavenumber 1704–1699 cm^{-1} in comparison with free EXN (1690 cm^{-1}). According to these assignments, the nitrogen atom in the piperazyl ring allows the EXN medication to function as an unidentate chelate. The existence of new absorption bands in the 2700–2400 cm^{-1} range is attributed to the stretching vibrations of water molecules crystallizing due to hydrogen bond effects. It is implied that there is no cooperation between metal ions and oxygen atoms since the $\nu(OH)_{COOH}$ vibration changes very little. Hydrogen bonding also broadens the O-H stretch of carboxylic acids and is linked to two distinct infrared stretching absorptions that exhibit significant changes in response to hydrogen bonding. The assignments of the other stretching vibration motions ν(M–N) vibrations in Ru(III), Pt(IV) and Ir(III)–EXN complexes **1-3** are observed at 493–418 cm^{-1} [34].

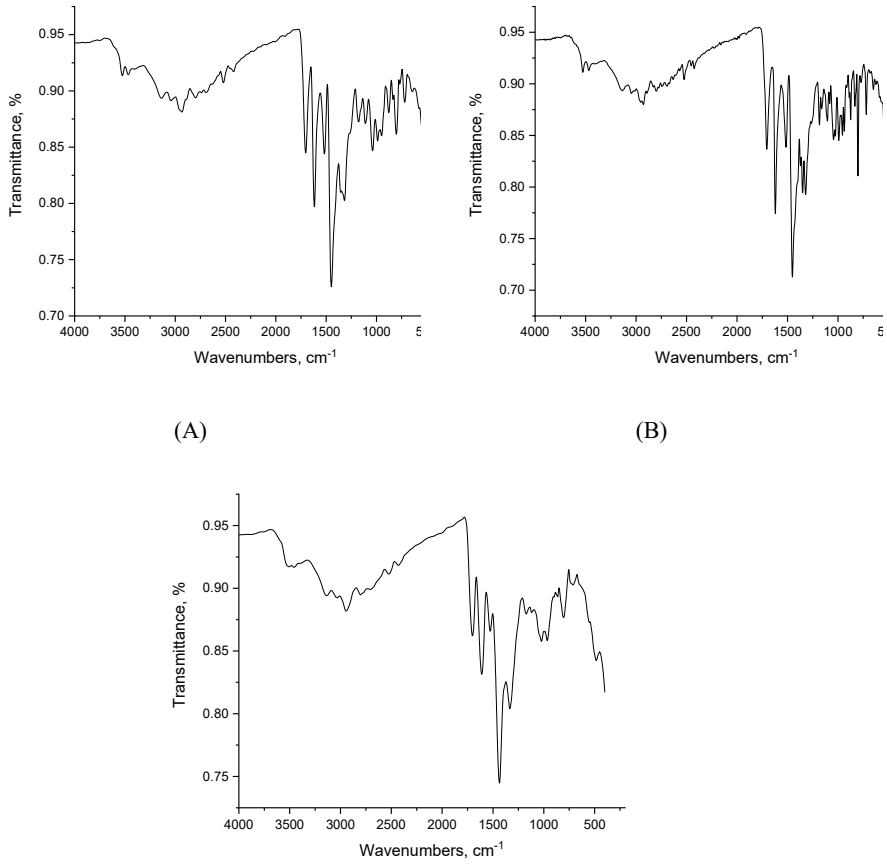

Figure 2. Infrared spectra of A: Ir(III)-EXN, B: Pt(IV)-EXN and C: Ru(III)-EXN complexes.

Table 1. FT–IR assignments of Ru^{3+}, Pt^{4+} and Ir^{3+}–EXN complexes.

Compounds	Assignments (cm^{-1})					
	$\nu(O–H)_{COOH}$	$\nu(C=O)_{COOH}$	$\nu(C=O)_{pyridone}$	$\delta(C–H)_{aromatic}$	$\nu(N–H)_{piperazyl}$	$\nu(M–N)$
EXN	3459	1690	1620	885	2970	-
Pt(IV) complex	3529 3469	1704	1618	872	-	493 468 418
Ru(III) complex	3524 3459	1699	1617	872	-	488
Ir(III) complex	3529 3469	1704	1613	877	-	488 418

Electronic spectra and magnetic measurements

The Ru(III), Pt(IV), and Ir(III)-EXN complexes **1-3** with 10^{-3} M in DMSO solvent were scanned for electronic UV–Vis spectra in the 800-200 nm region. These three novel EXN compounds' spectra show some distinct bands at 250–300 nm, 300–350 nm, and 350–450 nm within three regions. According to existing research, the first range can be attributed to the electronic transition between π→π* for aromatic hydrocarbon rings. The second range contains some electronic absorption bands that are associated with the n→π* transition for ketonic, NH imine, and carboxylic groups and the third range is linked to the d-d transition M-L_{CT}, respectively [35-40].

Table 2 lists the ruthenium(III)-EXN complex's electronic spectrum values in solid sample. Ru(III) has a ground state of ^2T2_g. It is known that the $t_{2g}\ ^4e_{1g}$ configuration gives rise to the initial excited doublet levels, $^2A_{2g}$ and $^2T_{1g}$, in ascending order of energy [35-38]. In increasing order of energy, the Ru(III) complex exhibits three electronic transitions at 22573 cm^{-1}, 27933 cm^{-1}, and 29762 cm^{-1}. These transitions can be attributed to $^2T_{2g}\rightarrow{}^4T_{1g}$ (ν1), $^2T_{2g}\rightarrow{}^4T_{2g}$ (ν2), and $^2T_{2g}\rightarrow{}^2A_{2g}$ (ν3). The following equations (1-3) [38-40] were used to compute the ligand field parameters (10 Dq) and the interelectronic repulsion parameters (B and C):

$$^2T_{2g}\rightarrow{}^4T_{1g}\ (\nu1) = 10\ Dq - 5B - 4C \quad (1)$$

$$^2T_{2g}\rightarrow{}^4T_{2g}\ (\nu2) = 10\ Dq + 3B - 4C \quad (2)$$

$$^2T_{2g}\rightarrow{}^2A_{2g}\ ,\ ^2T_{1g}\ (\nu3) = 10\ Dq - 2B - C \quad (3)$$

The ligand field parameter values are similar among the several ruthenium(III) complexes documented in the literature [40]. The complex's measured Racah interelectronic repulsion parameter (B) is smaller than that of the Ru(III) ion (B' = 630 cm^{-1}) [39, 40]. With a nephelauxetic parameter (β = B/B') ≤ 1.0, the 10Dq value is high. A decrease in the β value is similarly linked to a decrease in the metal ion's effective positive charge and an increasing propensity to reduce to the lower oxidation state [39]. These findings imply that the EXN donor and Ru(III) ions have a strong covalent connection [34-38]. Reliability of ruthenium(III)-EXN complex (**2**) to magnetic fields at room temperature was measured with a Gouy magnetic balance. The ruthenium(III) complex has a paramagnetic property with S = ½ and d^5 (low spin). The ruthenium(III) complex's magnetic moment of 1.99 B.M. supports the observation of a single unpaired electron in an octahedral environment for the Ru(III) ion in a low spin $4d^5$ configuration [39, 40].

Charge-transfer transitions in the electronic spectra of the platinum(IV) complex (**1**) may interfere and make it impossible to observe all of the predicted bands [39]. The unique bands at 33784 cm^{-1} and 30030 cm^{-1} cans be attributed to a combination of the d-d transition band and metal ligand charge transfer (M→L_{CT}). The combination of d-d transition bands and N→Pt(IV) metal charge transfer (Lπ→Pt_{CT}) is responsible for the other weak band at 27933 cm^{-1}. Given that the Pt(IV) complex 1 exhibits diamagnetic property, the platinum(IV) complex's geometry must be octahedral. Four bands are anticipated as a result of the $^1A_{1g}\rightarrow{}^3T_{1g}$, $^1A_{1g}\rightarrow{}^3T_{2g}$, and $^1A_{1g}\rightarrow{}^1T_{1g}$ and $^1A_{1g}\rightarrow{}^1T_{2g}$ transitions in the Pt(IV) d^6 system. Following complexation, the interaction between the nitrogen atom of the piperazyl ring and the Pt(IV) ion causes a shift in frequency to a lower value.

The character of the iridium(III) complex **3** is diamagnetic. The spectrum from UV to Vis of iridium(III) complex 3 exhibits bands at 30030 cm^{-1} and 33670 cm^{-1}. From the ground state $^1A_{1g}$, these two bands were inferred. They were found in the predicted ranges [34-38] for the two spin-allowed transitions, $^1A_{1g}\rightarrow{}^1T_{1g}$ (ν1) and $^1A_{1g}\rightarrow{}^1T_{2g}$ (ν2). In the Ir(III) complex 3, the ratio ν2/ν1 is 1.1212, in agreement with the octahedral geometry for iridium(III) complexes reported in the literature [38-40]. Based on the following equations (4 and 5) [39, 40], the ligand field parameters 10Dq and nephelauxetic (B) have been computed using the $^1A_{1g}\rightarrow{}^1T_{1g}$ (ν1) and $^1A_{1g}\rightarrow{}^1T_{2g}$ (ν2) transitions:

$$\nu1 = 10Dq - 4B + \frac{86(B)^2}{10Dq} \quad (4)$$

$$\nu2 = 10Dq + 12B + \frac{2(B)^2}{10Dq} \quad (5)$$

The ν2/ν1, 10Dq, B, C, and β parameters' outcome values accord with those of other iridium(III) complexes from earlier research [39, 40]. In the Ir(III) complexes, the B value corresponds to approximately 34% of the free iridium ion (660 cm^{-1}) and denotes the considerable covalency overlap in the metal ligand σ-bond.

Table 2. Electronic spectral bands (cm^{-1}) and ligand field parameters of Ru^{3+}, Pt^{4+} and Ir^{3+}–EXN complexes.

Complex	λ_{max} (cm^{-1})	Assignments	ν2/ν1	10Dq (cm^{-1})	B (cm^{-1})	C (cm^{-1})	β
Pt(IV)	27933 30030 33784	$^1A_{1g}\rightarrow{}^3T_{1g}$ $^1A_{1g}\rightarrow{}^3T_{2g}$ $^1A_{1g}\rightarrow{}^1T_{1g}$ & $^1A_{1g}\rightarrow{}^1T_{2g}$	-	-	-	-	-
Ru(III)	22573 27933 29762	$^2T_{2g}\rightarrow{}^4T_{1g}$(ν1) $^2T_{2g}\rightarrow{}^4T_{2g}$(ν2) $^2T_{2g}\rightarrow{}^2A_{2g}$, $^2T_{1g}$ (ν3)	1.2374	23895	670	507	1.06
Ir(III)	30030 33670	$^1A_{1g}\rightarrow{}^1T_{1g}$ (ν1) $^1A_{1g}\rightarrow{}^1T_{2g}$ (ν2)	1.1212	30940	227	908	0.344

^1H NMR spectra

Important Information ^1H NMR signals of enoxacin are detected at chemical shifts of 1.40 (3H, $–CH_3$ methyl), 2.0 (1H, amine), 2.62 (4H, piperazine), 3.85 (4H, piperazine), 4.48 (2H, $–CH_2–$ ethyl), and 8.10, 8.95 (2H, naphthyridine) [41].

Since the aliphatic and piperazine protons share the same binding site with the ligand, it is noticed that the signals for these protons are altered when comparing the major peaks of enoxacin with its complexes. The piperazine ring's NH proton, which is present in free EXN-free medication at 2.0 ppm, is absent. However, in the platinum(IV) complex spectrum (Figure 3), the resonance of the naphthyridine proton from 8.10–8.95 occurred upfield near 7.41–8.65 ppm. The absence of the carboxylic proton (COOH) resonance in the Pt(IV) complex spectrum indicates that the oxygen atoms in the ketonic group of the pyridone ring of enoxacin and the proton of carboxylic acid form an intermolecular hydrogen bond. Because coordinated water molecules are present, the OH proton peak appears at 3.50 ppm, next to the piperazine protons. Our research indicates that enoxacin interacts with the metal center through the deprotonated of amine proton of piperazine, functioning as a monoanionic monodentate ligand. Based on the acquired data, the Ru(III), Ir(III), and Pt(IV) complexes are hypothesized to be six coordinate, with three enoxacin molecules chelating the center metal atom from three sides and two water molecules and chloride ion at the octahedron's chelates (Figure 1).

Thermal analyses

The formulae for the Ru(III), Ir(III), and Pt(IV)-EXN complexes **1–3** presented in this paper were determined using thermogravimetric analysis (TG) and differential thermogravimetric analysis (DTG). As seen in Figures 4a–c, TGA and DTG thermograms are carried out under N_2 flow. For every synthesized complex, For the EXN complexes **1–3**, the temperature data allowed us to determine the number of crystallized water molecules outside/inside of the coordination sphere. The breakdown of $[Ru(EXN)_3(H_2O)_3]$ at high temperatures (Figure 4a) take place at three primary

degradation stages which are roughly at 59-182 °C, 182-369 °C, and 369-795 °C, respectively. The weight loss linked to these phases is 77.75%, which is extremely near to the calculated theoretical value of 77.27%, which denotes the loss of three EXN and three coordinated water molecules. The RuO_2 contaminated with few carbon atoms (found, 22.25%; theoretical, 22.73%) is the final thermal product obtained at 800 °C. The $[Ir(EXN)_3(H_2O)_3]$ thermal breakdown (Figure 4b) show the three primary stages of the degradation of the iridium(III) complex. Three coordinated water molecules are lost during the first stage of decomposition, which starts at a maximum temperature of 86-212 °C and results in a weight loss of 2.65%. At maximum temperatures of 212-360 °C, 360-493 °C and 493-795 °C, respectively, the second, third and fourth stages of decomposition take place. Three EXN molecules are lost during these phases, resulting in a weight loss of 83.63%. Following breakdown, the residue's weight was found to be 13.91%, which corresponds to an actual total weight loss of 16.71%, as per our calculations. Iridium metal is the byproduct of thermal breakdown. Four stages of thermal degradation at 179-312 °C, 312-402 °C, 402-633 °C, and 633-792 °C are seen in the $[Pt(EXN)_3(H_2O)_2Cl]$ complex, as illustrated in Figure 4c. Due to its anhydrous nature, the complex undergoes a first stage of decomposition at a high maximum temperature of 179 °C. As a result, the complex begins to decompose at this DTG_{max} and continues to do so through the second, third and fourth stages, resulting in a total weight loss of 43.82%, which is equivalent to the loss of three EXN, two coordinated water molecules and one chlorine atom, which, in theory, correspond to a weight loss of 43.57%. The weight of the remnant (Pt metal) contaminated with carbon atoms after final decomposition is 56.18% (theoretically 56.44%), which agrees with our computed total weight loss figure of 43.82% for the actual weight loss.

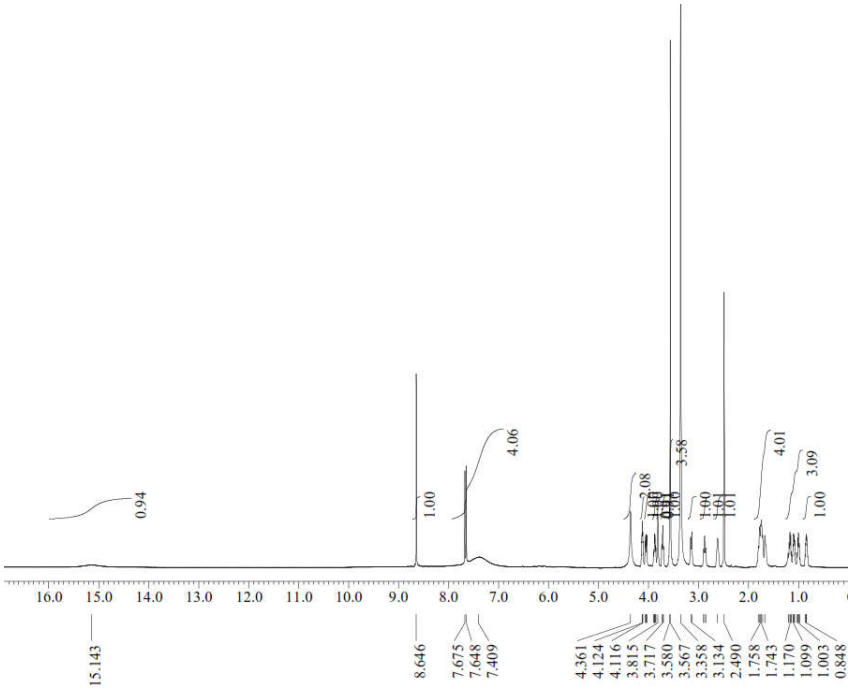

Figure 3. ^{1}H NMR spectrum of Pt(IV)-EXN complex.

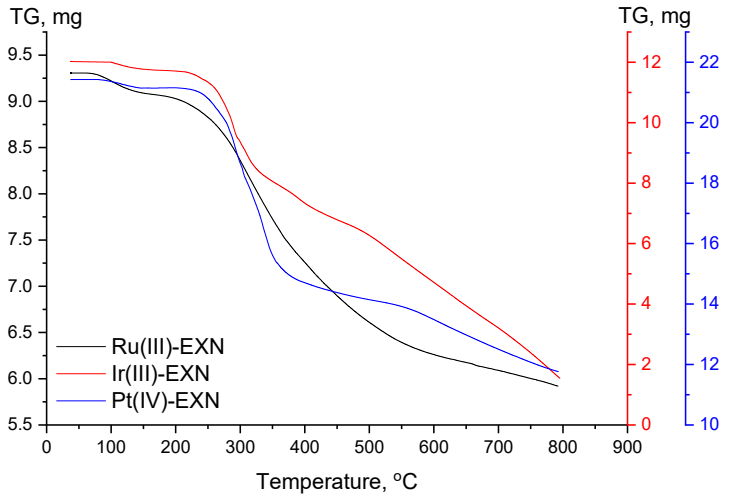

Figure 4. TGA and DrTGA curves of Ru(III)-EXN, Ir(III)-EXN, and Pt(IV)-EXN complexes.

X-Ray powder diffractions

Figure 5a-c displays the X-ray solid powder diffractions of the complexes $[Pt(EXN)_3(H_2O)_2Cl]$ (**1**), $[Ru(EXN)_3(H_2O)_3]$ (**2**), and $[Ir(EXN)_3(H_2O)_3]$ (**3**). These patterns of diffraction are semicrystalline. Using the Deby-Scherrer formula, the particle size (D) of EXN complexes 1-3 was calculated based on the principal diffraction patterns of each complex [42], where K is defined as 0.94, β is the full width at half maximum (FWHM, β) of the prominent intensity peak (100% relative intensity peak), and θ is the peak position, λ is the wavelength of the X-ray (1.5418 Å) for Cu Kα radiation. Using the Deby-Scherrer formula, the grain sizes for the Ru(III), Ir(III), and Pt(IV) complexes were determined to be 6, 8, and 5 nm, respectively. The growing EXN chelates surrounding metal ions (ratio 1:3) can be used to explain the smaller particle size [43]. Table 3 lists the XRD data that was gathered, including 2θ, intensities, and d spacing. Table 3 lists the dislocation density (δ), which was calculated using the following equations (6 and 7) [44] and shows the development of high-quality complexes.

$$D = \frac{K\,\lambda}{\beta \cos\theta} \qquad (6)$$

$$\delta = \frac{1}{D^2} \qquad (7)$$

Table 3. The XRD collected data of crystallite sizes (D), dislocation density (δ), 2θ, intensities, and d-spacing of Ru(III), Ir(III), and Pt(IV) complexes.

Complex	D (nm)	δ (10^{12}.lin.m^{-2})	2Theta	Intensity	d-Spacing
Ru(III)	6	0.0278	32	100	2.7508
Ir(III)	8	0.0156	32	100	2.7507
Pt(IV)	5	0.0400	32	100	2.7478

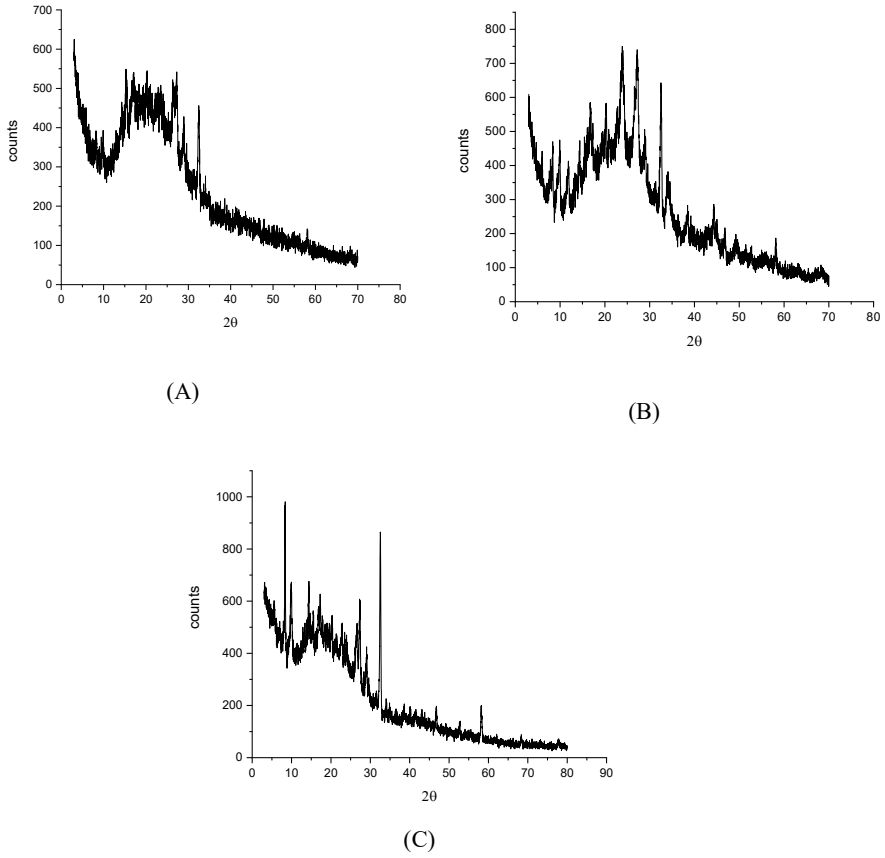

Figure 5. XRD spectra of A: Ir(III)-EXN, B: Pt(IV)-EXN and C: Ru(III)-EXN complexes.

SEM and TEM morphology

Here, the surface morphology and particle size of the Ru(III), Ir(III), and Pt(IV)-EXN complexes are examined using scanning electron microscopy pictures, which show crystalline and irregular structures. The micrograph's layers show that the system's atoms are arranged in a clearly defined pattern, indicating that all the reactants have fully reacted to form a single, homogenous molecule. On average, the SEM image displays a single-phase development with distinct grain characteristics and particle sizes between 5 and 200 μm. The TEM images of EXN complexes verify the existence of NPs that are spherical or semispherical and seem like dark dots.

Antibacterial assessments

Bacteria G(+) (*Bacillus subtilis* and *Staphylococcus Aureus*) and G(-) (*Pseudomonas aeruginosa* and *Escherichia coli*) were the four types of bacteria used to evaluate the antibacterial efficacy of enoxacin complexes containing Ru(III), Pt(IV), and Ir(III). The test samples' inhibition zone diameters are compiled and added to Table 4. Compared to the common antibiotic Ampicillin,

the three EXN complexes exhibit greater antibacterial efficacy against all strains of microorganisms, including *Bacillus subtilis*, *Staphylococcus aureus*, *Pseudomonas aeruginosa*, and *Escherichia coli*.

The type of strain of microorganisms:

Name	Gram reaction	ATCC
Bacillus subtilis	G^+	6051
Escherichia coli	G^-	11775
Pseudomonas aeruginosa	G^-	10145
Staphylococcus aureus	G^+	12600

In comparison to ligand and conventional medications, the ruthenium(III), platinum(IV), and iridium(III) complexes had superior inhibitory effects and antibacterial properties. Tweedy's chelation provides an explanation for this, since it reduces the polarity of the metal cation due to partial sharing of the metal ion's positive charge and ligand orbital overlap. Additionally, the chelation increases the p-electrons' delocalization over the chelate ring, which raises the lipophilicity. This causes a spike in the penetration of complexes into lipid membranes, which blocks the target microorganisms' enzymes' metal sites. Additionally, the metal complexes prevent protein synthesis and cell respiration, which hinders the growth of microorganisms [45].

Table 4. Antibacterial activities of EXN complexes.

Sample	Inhibition zone diameter (mm/mg sample)			
	Bacterial species			
	G^+		G^-	
	Bacillus subtilis	*Staphylococcus aureus*	*Escherichia coli*	*Pseudomonas aeruginosa*
Control: DMSO	0.0	0.0	0.0	0.0
Standard: Ampicillin Antibacterial agent	26	21	25	26
Ir(III)	34	38	31	36
Pt(IV)	36	39	31	37
Ru(III)	32	36	30	33

G: Gram reaction. Solvent: DMSO.

Anticancer assessments

In *vitro* cytotoxicity tests were performed on human breast cancer cell line MCF-7 and human hepatocellular carcinoma cell line HepG-2 to evaluate the effects of enoxacin complexes of Ru(III), Pt(IV), and Ir(III) metal ions in comparison to two commonly used anticancer drugs, doxrubcin and cisplatin. Figure 6 shows the findings on inhibitory activities that were evaluated using the IC_{50} inhibitory concentration calculation. The platinum(IV) complex exhibits a higher IC_{50} against the HepG-2 cell line compared to the ruthenium(III) and iridium(III) complexes, but the iridium(III) complex outperforms the platinum(IV) and ruthenium(III) complexes against the MCF-7 cell line.

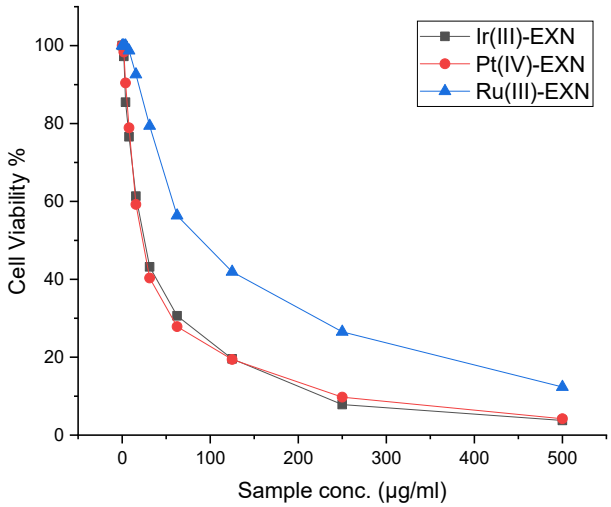

Figure 6a. Evaluation of cytotoxicity of Ir(III) (IC_{50} = 25.4±1.9 µg/ml), Pt(IV) (IC_{50} = 23.2±1.2 µg/ml), and Ru(III)-EXN (IC_{50} = 90±4.5 µg/ml) complexes against HepG-2 cell line.

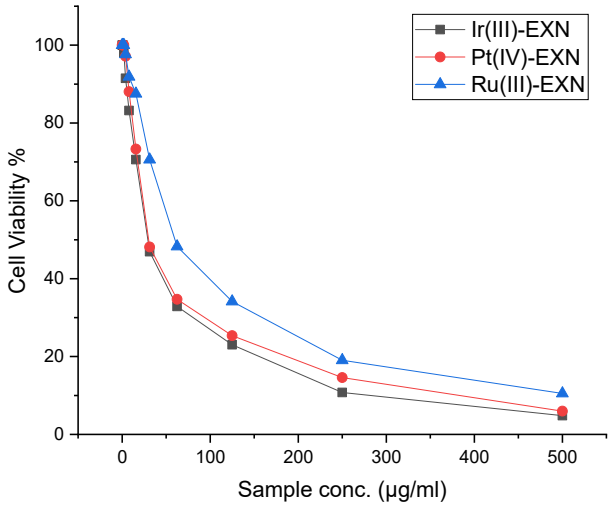

Figure 6b. Evaluation of cytotoxicity of Ir(III) (IC_{50} = 29.2±1.8 µg/mL), Pt(IV) (IC_{50} = 30.1±1.8 µg/mL), and Ru(III)-EXN (IC_{50} = 60.1±3.9 µg/mL) complexes against MCF-7 cell line.

ACKNOWLEDGEMENT

Princess Nourah bint Abdulrahman University Researchers Supporting Project number (PNURSP2024R75), Princess Nourah bint Abdulrahman University, Riyadh, Saudi Arabia.

CONCLUSION

The interaction of fluoroquinolone drug enoxacin (EXN) with platinum(IV), ruthenium(III), and iridium(III) chlorides was investigated. Solid complexes, obtained as products of this interaction, were isolated and characterized by elemental analysis, spectral (FTIR, ^{1}H-NMR, electronic, and XRD) and electron microscope (SEM) analysis measurements. The spectral studies of the isolated complexes suggest that EXN act as monodentate ligand that bind through N atom of the piperazine ring. The obtained results indicate the formation of the complexes of the following formulas: $[Pt(EXN)_3(H_2O)_2Cl]$, $[Ru(EXN)_3(H_2O)_3]$, and $[Ir(EXN)_3(H_2O)_3]$. HepG-2 (human hepatocellular carcinoma) and MCF-7 (human breast cancer cell line) were used to analyze the results of in *vitro* cytotoxicity against Pt(IV), Ru(III), and Ir(III) complexes.

REFERENCES

1. Macias, B.; Villa, M.V. Rubio, I.; Castineiras, A.; Borras, J. Complexes of Ni(II) and Cu(II) with ofloxacin: Crystal structure of a new Cu(II) ofloxacin complex. *J. Inorg. Biochem*. **2001**, 84, 163–170.
2. Robles, J.; Martin-Polo, J.; Alvarez-Valtierra, L.; Hinojosa, L.; Mendoza, G.D. A theoretical-experimental study on the structure and activity of certain quinolones and the interaction of their Cu(II)-complexes on a DNA model. *Met.-Based Drugs* **2000**, 7, 301–311.
3. Ehimiadou, E.K.; Sanakis, Y.; Katsarou, M.; Raptopoulou, C.P.; Karaliota, A.; Katsaros, I.; Psomas, G. Neutral and cationic mononuclear copper(II) complexes with enrofloxacin: Structure and biological activity. *J. Inorg. Biochem*. **2006**, 100, 1378–1388.
4. Lipunova, G.; Nosova, E.; Charushin, V. Metallocomplexes of fluoroquinolonecarboxylic acids. *Russ. J. Gen. Chem*. **2009**, 79, 2753–2766.
5. Saraiva, R.; Lopes, S.; Ferreira, M.; Novais, F.; Pereira, E.; Feio, M.J.; Gameiro, P. Solution and biological behaviour of enrofloxacin metalloantibiotics: a route to counteract bacterial resistance?. *J. Inorg. Biochem*. **2010**, 104, 843–850.
6. Seran, A.; Stanczak, A. The complexes of metal ions with fluoroquinolones. *Russ. J. Coord. Chem*. **2009**, 35, 81–95.
7. Wu, G.G.; Wang, G.P.; Fu, X.C.; Zhu, L.G. Synthesis, crystal structure, stacking effect and antibacterial studies of a novel quaternary copper(II) complex with quinolone. *Molecules* **2003**, 8, 287–296.
8. Chen, C.Y.; Chen, Q.Z.; Wang, X.F.; Liu, M.S.; Chen, Y.F. Synthesis, characterization, DNA binding properties, and biological activities of a mixed ligand copper(II) complex of ofloxacin. *Trans. Met. Chem*. **2009**, 34, 757–763.
9. Sheikhshoaie, I.; Ebrahimipour, S.Y.; Lotfi, N.; Mague, J.T.; Khaleghi, M. Synthesis, spectral characterization, X-ray crystal structure and antimicrobial activities of two cis dioxido-vanadium(V) complexes incorporating unsymmetrical dimalonitrile-based (NNO) Schiff base ligands. *Inorg. Chim. Acta* **2016**, 442, 151–157.
10. Elsayed, S.A.; Badr, H.E.; di Biase, A.; El-Hendawy, A.M. Synthesis, characterization of ruthenium(II), nickel(II), palladium(II), and platinum(II) triphenylphosphine-based complexes bearing an ONS-donor chelating agent: Interaction with biomolecules, antioxidant, in vitro cytotoxic, apoptotic activity and cell cycle analysis. *J. Inorg. Biochem.* **2021**, 223, 111549.
11. Devasia, J.; Chinnam, S.; Khatana, K.; Shakya, S.; Joy, F.; Rudrapal, M.; Nizam, A. Synthesis, DFT and in silico anti-COVID evaluation of novel tetrazole analogues. *Polycycl. Aromat. Comp.* **2023**, 43, 1941–1956.
12. Hussen, N.H.; Hasan, A.H.; Jamalis, J.; Shakya, S.; Chander, S.; Kharkwal, H.; Murugesan, S.; Bastikar, V.A.; Gupta, P.K.P. Potential inhibitory activity of phytoconstituents against

black fungus: *In silico* ADMET, molecular docking and MD simulation studies. *Comput. Toxicol.* **2022**, 24, 100247.
13. Hasan, A.H.; Shakya, S.; Hussain, F.H.S.; Murugesan, S.; Chander, S.; Pratama, M.R.F.; Jamil, S.; Das, B.; Biswas, S.; Jamalis, J. Design, synthesis, anti-acetylcholinesterase evaluation and molecular modelling studies of novel coumarin-chalcone hybrids. *J. Biomol. Struct. Dyn.* **2023**, 41, 11450–11462.
14. Franz, K.J.; Metzler-Nolte, N. Introduction: Metals in medicine. *Chem. Rev*. **2019**, 119, 727–729.
15. Zhang, C.X.; Lippard, S.J. New metal complexes as potential therapeutics. *Curr. Opin. Chem. Biol*. **2003**, 7, 481–489.
16. Zou, T.; Lum, C.T.; Lok, C.-N.; Zhang, J.-J.; Che, C.-M. Chemical biology of anticancer gold(III) and gold(I) complexes. *Chem. Soc. Rev*. **2015**, 44, 8786–8801.
17. Coverdale, J.P.C.; Laroiya-McCarron, T.; Romero-Canelon, I. Designing ruthenium anticancer drugs: What have we learnt from the key drug candidates?. *Inorganics* **2019**, 7, 31.
18. Manivel, J.; Sangeetha, S.; Murali, M. DNA and BSA interaction, DNA cleavage and in vitro cytotoxicity of copper(II) complexes: [Cu(bba)(phen)]$(ClO_4)_2$ is Promising chemotherapeutic scaffold. *J. Sci. Res*. **2020**, 12, 111–133.
19. Ndagi, U.; Mhlongo, N.; Soliman, M.E. Metal complexes in cancer therapy–an update from drug design perspective. *Drug Des. Dev. Ther*. **2017**, 11, 599–616.
20. Cozzarelli, N.R. DNA gyrase and the supercoiling of DNA. *Science* **1980**, 207, 953–960.
21. Sha, J.Q.; Li, X.; Qiu, H.B.; Zhang, Y.H.; Yan, H. Nickel complexes of the different quinolone antibacterial drugs: Synthesis, structure and interaction with DNA. *Inorg. Chim. Acta* **2012**, 383, 178–184.
22. Sousa, E.; Graca, I.; Baptista, T.; Vieira, F. Q.; Palmeira, C.; Henrique, R.; Jeronimo, C. Enoxacin inhibits growth of prostate cancer cells and effectively restores microRNA processing. *Epigenetics* **2013**, 8, 548–558.
23. Chen, Z.F.; Yu, L.C.; Zhong, D.C.; Liang, H.; Zhu, X.H.; Zhou, Z.Y. Cu(II) and Co(II) ternary complexes of quinolone antimicrobial drug enoxacin and levofloxacin: structure and biological evaluation. *Inorg. Chem. Commun*. **2006**, 4, 9839–9843.
24. Ehimiadou, E.K.; Sanakis, Y.; Raptopoulou, C.P.; Karaliota, A.; Katsaros, N.; Psomas, G. Crystal structure, spectroscopic, and biological study of the copper(II) complex with third-generation quinolone antibiotic sparfloxacin. *Bioorg. Med. Chem. Lett*. **2006**, 16, 3864–3867.
25. Liu, Y.C.; Chen, Z.F.; Shi, S.M.; Luo, H.S.; Zhong, D.C.; Zou, H.L.; Liang, H. Synthesis, crystal structure of polyoxovanadate complex of ciprofloxacin: $V_4O_{10}(\mu 2\text{-}O)_2$[VO(H-Ciprof) 2]$_2\cdot 13H_2O$ by hydrothermal reaction. *Inorg. Chem. Commun*. **2007**, 10, 1269–1272.
26. Yu, L.C.; Tang, Z.L.; Yi, P.G.; Liu, S.L. Hydrothermal syntheses, crystal structures and antibacterial activities of two transition metal complexes with ciprofloxacin. *J. Coord. Chem*. 2009, 62, 894–902.
27. Tarushi, A.; Psomas, G.; Raptopoulou, C.P.; Kessissoglu, D.P. Zinc complexes of the antibacterial drug oxolinic acid: Structure and DNA-binding properties. *J. Inorg. Biochem*. **2009**, 103, 898–905.
28. Saha, D.K.; Sandbhor, U.; Shirisha, K.; Padhye, S.; Deobagkar, D.; Anson, C.E.; Powell, A.K. A novel mixed-ligand antimycobacterial dimeric copper complex of ciprofloxacin and phenanthroline. *Bioorg. Med. Chem. Lett*. **2004**, 14, 3027–3032.
29. Efthimiadou, E.K.; Katsarou, M.E.; Sanakis, Y.; Raptopoulou, C.P.; Karaliota, A.; Katsaros, N.; Psomas, G. Neutral and cationic mononuclear copper(II) complexes with enrofloxacin: Structure and biological activity. *J. Inorg. Biochem*. **2006**, 100, 1378–1388.
30. Efthimiadou, E.K.; Thomadaki, H.; Sanakis, Y.; Raptopoulou, C.P.; Katsaros, N.; Scorilas, A.; Karaliota, A.; Psomas, G. Structure and biological properties of the copper(II) complex

with the quinolone antibacterial drug *N*-propyl-norfloxacin and 2,2′-bipyridine. *J. Inorg. Biochem*. **2007**, 101, 64–73.
31. Oyedemi, S.O.; Bradley, G.; Afolayan, A.J. Anticabterial and antioxidant activities of hydroalcoholic stem bark extract of *Schotia latifolia* Jacq. *Asian Pac. J. Trop. Med.* **2011**, 4, 952–958.
32. Geary, W.J. The use of conductivity measurements in organic solvents for the characterisation of coordination compounds. *Coord. Chem. Rev*. 1971, 7, 81–122.
33. Yang, L.; Li, W.; Tao, D.; Li, Y.; Yang, X. Synthesis and characterization of main group metal complexes with pipemedic acid. *Synth. React. Inorg. Met.-Org. Chem*. **1999**, 29, 1485–1494.
34. Alghamdi, M.T.; Alsibaai, A.A.; Shahawi, M.S.; Refat, M.S. Synthesis and spectroscopic studies of levofloxacin uni-dentate complexes of Ru(III), Pt(IV) and Ir(III): Third generation of quinolone antibiotic drug complexes. *J. Mol. Liq*. **2016**, 224 Part A, 571-579.
35. Alghamdi, M.T.; Alsibaai, A.A.; Shahawi, M.S.; Refat, M.S. Structural and chelation behaviors of new Ru(III), Pt(IV) and Ir(III) gatifloxacin drug complexes: Spectroscopic characterizations. *J. Mol. Struct*. **2017**, 1130, 264–275.
36. Alibrahim, K.A.; Al-Saif, F.A.; Alghamdi, M.T.; El-Shahawi, M.S.; Moustafa, Y.M.; Refat, M.S. Synthesis, spectroscopic, thermal, antimicrobial and electrochemical characterization of some novel Ru(III), Pt(IV) and Ir(III) complexes of pipemidic acid. *RSC Adv.* **2018**, 8, 22515–22529.
37. Alibrahim, K.A.; Al-Saif, F.A.; Alghamdi, M.T.; El-Shahawi, M.S.; Althubeiti, K.; Aljuhani, E.; Refat, M.S. Spectroscopic, molecular structural, thermal, biological and voltammetric characterization of Ru^{3+}, Pt^{4+} and Ir^{3+} complexes of lomefloxacin drug. *Lat. Am. J. Pharm*. **2019**, 38, 1077–1090.
38. Alosaimi, E.H.; Alsibaai, A.A.; El-Shahawi, M.S.; Refat, M.S. Synthesis, physicochemical and thermal analyses of Ru(III), Pt(IV) and Ir(III) complexes with NO bidentate Schiff base ligand. *Russ. J. Phys. Chem. A* **2018**, 92, 2227–2236.
39. Lever, A.B. *Inorganic Electronic Spectroscopy*, Elsevier: Amsterdam; **1968**.
40. Figgis, B.N. *Introduction to Ligand Field Theory*, 1st ed., Interscience Publishers: New York; **1967**, p. 287.
41. Arayne, S.; Sultana, N.; Haroon, U.; Mesaik, M.A. Synthesis, characterization, antibacterial and anti-inflammatory activities of enoxacin metal complexes. *Bioinorg. Chem. Appl.* **2009**, 2009, 914105.
42. Cullity, B.D. *Elements of X-ray Diffraction*. Addison-Wesley: Reading, MA; **1972**, p. 102.
43. Salavati-Niasari, M.; Mohandes, F.; Davar, F.; Mazaheri, M.; Monemzadeh, M.; Yavarinia, N. Preparation of NiO nanoparticles from metal-organic frameworks via a solid-state decomposition route. *Inorg. Chim. Acta* **2009**, 362, 3691–3697.
44. Velumani, S.; Mathew, X.; Sebastian, P.J. Structural and optical characterization of hot wall deposited CdSexTe1−x films. *Solar Energy Mater. Solar Cells* **2003**, 76, 359–368.
45. Pasdar, H.; Foroughifar, N.; Davallo, M.; Davallo, M. Synthesis, characterization and antibacterial activity of novel 1,3-diethyl-1,3-bis(4-nitrophenyl) urea and its metal(II) complexes. *Molecules* **2017**, 22, 2125.